Journal Pre-proof

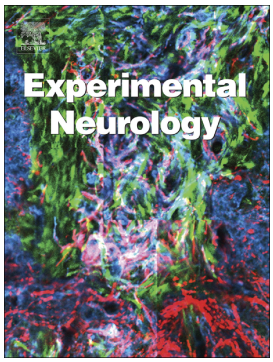

A novel pyrazolo [3,4-d] pyrimidine, KKC080106, activates the Nrf2 pathway and protects nigral dopaminergic neurons

Ji Ae Lee, Hye Ri Kim, Hyo Jin Son, Nari Shin, Se Hee Han, Chan Sung Chung, Dong Jin Kim, Onyou Hwang

PII: S0014-4886(20)30218-1

DOI: https://doi.org/10.1016/j.expneurol.2020.113387

Reference: YEXNR 113387

To appear in: *Experimental Neurology*

Received date: 9 December 2019

Revised date: 20 May 2020

Accepted date: 18 June 2020

Please cite this article as: J.A. Lee, H.R. Kim, H.J. Son, et al., A novel pyrazolo [3,4-d] pyrimidine, KKC080106, activates the Nrf2 pathway and protects nigral dopaminergic neurons, *Experimental Neurology* (2020), https://doi.org/10.1016/j.expneurol.2020.113387

A novel pyrazolo [3,4-*d*] pyrimidine, KKC080106, activates the Nrf2 pathway and protects nigral dopaminergic neurons

Ji Ae Lee[a], Hye Ri Kim[a], Hyo Jin Son[a], Nari Shin[a], Se Hee Han[a], Chan Sung Chung[b], Dong Jin Kim[b,*], Onyou Hwang[a,*]

[a]Department of Biochemistry and Molecular Biology, University of Ulsan College of Medicine, Seoul, South Korea

[b]Center for Neuro-Medicine, Brain Science Institute, Korea Institute of Science and Technology, Seoul, South Korea

*Corresponding authors: Onyou Hwang, Ph.D., Department of Biochemistry and Molecular Biology, University of Ulsan - College of Medicine, 88 Olympic-ro, 43-gil, Songpa-gu, Seoul 05505, South Korea.; TEL: 822-3010-4279; e-mail: oyhwang@amc.seoul.kr and Dong Jin Kim, Ph.D., Center for Neuro-Medicine, Brain Science Institute, Korea Institute of Science and Technology, 5 Hwarang-ro, 14-gil, Seongbuk-gu, Seoul 02792, South Korea; TEL: 822-958-5142; e-mail: djk2991@kist.re.kr

Abbreviations: MPTP, 1-methyl-4-phenyl-1,2,3,6-tetrahydropyridine; CDDO-Me, bardoxolone methyl; GCLC, catalytic subunit of GCL; COX-2, cyclooxygenase-2; DMSO, dimethyl sulfoxide; FBS, fetal bovine serum; GCL, glutamate cysteine ligase; GAPDH, glyceraldehyde 3-phosphate dehydrogenase; HO-1, heme oxygenase-1; iNOS, inducible NO synthase; IKK, IκB kinase; LDH, lactate dehydrogenase; LPS, lipopolysaccharide; GCLM, modifier subunit of GCL; NQO1, NAD(P)H:quinone oxidoreductase 1; NO, nitric oxide; Nrf2, nuclear factor-erythroid 2-related factor-2; PD, Parkinson's disease; RT, reverse transcription; SN, substantia nigra; TH, tyrosine hydroxylase

Abstract

The transcription factor nuclear factor-erythroid 2-related factor-2 (Nrf2) is known to induce neuroprotective and anti-inflammatory effects and is considered to be an excellent molecular target for drugs related to neurodegenerative disease therapy. Nrf2 activators previously tested in clinical trials were electrophilic, causing adverse effects due to non-selective and covalent modification of cellular thiols. In order to circumvent this issue, we constructed and screened a chemical library consisting of 241 pyrazolo [3,4-*d*] pyrimidine derivatives and discovered a novel, non-electrophilic compound: 1-benzyl-6-(methylthio)-*N*-(1-phenylethyl)-1*H*-pyrazolo[3,4-*d*]pyrimidine-4-amine (KKC080106). KKC080106 was able to activate Nrf2 signaling as it increases the cellular levels of Nrf2, binds to the Nrf2 inhibitor protein Keap1, and causes the accumulation of nuclear Nrf2. We also observed an increase in the expression levels of Nrf2-dependent genes for antioxidative/neuroprotective enzymes in dopaminergic neuronal cells. In addition, in lipopolysaccharide-activated microglia, KKC080106 suppressed the generation of the proinflammatory markers, such as IL-1β, TNF-α, cyclooxygenase-2, inducible nitric oxide synthase, and nitric oxide, and inhibited the phosphorylation of kinases known to be involved in inflammatory signaling, such as IκB kinase, p38, JNK, and ERK. As a drug, KKC080106 exhibited excellent stability against plasma enzymes and a good safety profile, evidenced by no mortality after the administration of 2,000 mg/kg body weight, and minimal inhibition of the hERG channel activity. Pharmacokinetic analysis revealed that KKC080106 has good bioavailability and enters the brain after oral and intravenous administration, in both rats and mice. In MPTP-treated mice that received KKC080106 orally, the compound blocked microglial activation, protected the nigral dopaminergic neurons from

degeneration, and prevented development of the dopamine deficiency-related motor deficits. These results suggest that KKC080106 has therapeutic potential for neurodegenerative disorders such as Parkinson's disease.

Keywords:
KKC080106; oxidative damage; neuroinflammation; neuroprotection; Parkinson's disease; Keap1

Introduction

Nuclear factor-erythroid 2-related factor-2 (Nrf2) is a transcription factor known to regulate cellular response to oxidative stress by inducing a number of antioxidative enzymes, including heme oxygenase-1 (HO-1), NAD(P)H:quinone oxidoreductase 1 (NQO1), and glutamate cysteine ligase (GCL) (Cuadrado et al., 2009). Nrf2 and its target gene products also play a role in the inflammation process as it decreases the production of proinflammatory mediators such as nitric oxide (NO), TNF-α, and IL-1β (Ahmed et al., 2017; Rojo et al., 2014). Nrf2 is normally present in the cytosol bound to its inhibitory protein Keap1. When exposed to stress conditions, Nrf2 is released from Keap1 and translocates into the nucleus where it binds to the antioxidant response element and induces the expression of its target genes (Lu et al., 2016). Therefore, the Nrf2/Keap1 signaling pathway is recognized as a suitable target that protects cells from oxidative and inflammatory stresses.

Parkinson's disease (PD) is a neurodegenerative disorder that causes movement deficits derived from an extensive loss of nigral dopaminergic neurons due to both oxidative and inflammatory damages. Accumulating evidence demonstrates that Nrf2 protects these neurons; for instance, the pathogenesis of idiopathic PD may be related to variations in the Nrf2 gene (von Otter et al., 2010; 2014) and dysregulation of the Nrf2 system has been observed in the brains of PD patients (Cook et al., 2011; Imaizumi et al., 2012). The absence of Nrf2 makes the nigral dopaminergic neurons more susceptible to oxidative stress (Lastres-Becker et al., 2012) and to various dopaminergic neurotoxins (Burton et al., 2006; Jakel et al., 2007; Innamorato et al., 2010). In animal models of PD, the absence of Nrf2 has been shown to exacerbate microglial activation

obtained by 1-methyl-4-phenyl-1,2,3,6-tetrahydropyridine (MPTP) (Rojo et al., 2010) and lipopolysaccharide (LPS) (Innamorato et al., 2008; 2010). Conversely, overexpression of Nrf2 provides neuroprotection in the MPTP mouse model (Chen et al., 2009), and activation of the Nrf2 signaling via Keap1 knockdown reduces oxidative stress and protects cells from MPTP-mediated neurotoxicity (Williamson et al., 2012).

Currently, the therapeutic interventions for PD are aimed only at mitigating the motor symptoms and cannot prevent or delay the underlying progression of the disease. Therefore, there is an urgent need for treatment that modifies the course of degeneration in PD. The well-known Nrf2 activators, bardoxolone methyl (CDDO-Me) and sulforaphane, have shown cytotoxicity in clinical trials resulting from off-target effects (Baier et al., 2014; de Zeeuw et al. 2013; Wang et al., 2014). Because these compounds are electrophilic, they can react indiscriminately with nucleophilic groups in cysteine thiols, which results in the depletion of cellular glutathione and in non-specific protein modifications (Abed et al., 2015; Kazoh and Lipton, 2017). Therefore, recent attention has been given to developing non-electrophilic compounds that could interfere with the Nrf2-Keap1 interaction (Schmoll et al., 2017).

Pyrazolo [3,4-*d*] pyrimidines are fused heterocyclic ring systems that form the central core of several more complex chemical compounds. With diverse biological activities, they have been implicated as potentially therapeutic (Chauhan and Kumar, 2013) and shown to interact with proteins (Schenone et al., 2014). In order to develop a novel Nrf2 activator, we have constructed and screened a library consisting of a series of synthetic analogs of pyrazolo [3,4-*d*] pyrimidine. Here, we report a novel non-electrophilic compound, KKC080106, which binds to Keap1, activates the Nrf2 signaling, provides neuroprotection, and exhibits good druggability.

Materials and Methods

Materials

Fetal bovine serum (FBS), horse serum, culture media, trypsin/EDTA, and penicillin-streptomycin were purchased from Thermo Fisher Scientific (Waltham, MA, USA). LPS, MPTP, dimethyl sulfoxide (DMSO), sulforaphane, sulfanilamide, naphthylethylenediamine dihydrochloride, CDDO-Me, and trypan blue dye were purchased from Sigma-Aldrich (St. Louis, MO, USA). The purified human 26S proteasome, Suc-Leu-Leu-Val-Tyr-AMC, Boc-Leu-Arg-Arg-AMC, Z-Leu-Leu-Glu-AMC, and MG-132 were purchased from Enzo Life Sciences (Farmingdale, NY, USA). First strand cDNA synthesis kit for RT-PCR was purchased from MBI Fermentas (Ontario, Canada), and CellTiter-Glo® Luminescent Cell Viability Assay kit was purchased from Promega (Madison, WI, USA). ELISA kits for IL-1β and TNF-α were obtained from R&D systems (Minneapolis, MN, USA) and eBioscience (San Diego, CA, USA), respectively. The recombinant His-tagged Keap1 protein was provided by Bioprogen (Daejeon, Korea). The antibodies used were: Nrf2, lamin B, the modifier subunit of GCL (GCLM), and IκB kinase (IKK) from Santa Cruz Biotechnologies (Santa Cruz, CA, USA); the catalytic subunit of GCL (GCLC) from Novus Biologicals (Littleton, CO, USA); HO-1 from Enzo Life Sciences; Iba-1 from Wako Chemicals (Osaka, Japan); HSP90, p-IKK, ERK, p-ERK, p38, p-p38, JNK and p-JNK from Cell Signaling Technology (Danvers, MA, USA); NQO1 from Ab Frontier (Seoul, Korea); tyrosine hydroxylase (TH) and β-actin from Sigma-Aldrich. Anti-rabbit IgG and anti-mouse IgG were purchased from Sigma-Aldrich. Vectastain ABC kit and biotinylated secondary antibodies were from Vector Laboratories (Burlingame, CA, USA). CHO-K1 Tet-On hERG cells were obtained from IonGate Biosciences GmbH (Frankfurt,

Germany), and the chemiluminescence detection system was from Pierce Chemical (Rockford, IL, USA). Chemicals used in organic synthesis were purchased from Sigma-Aldrich, Tokyo Chemical Industry (Tokyo, Japan), or Acros (Geel, Belgium). Ethyl acetate (EtOAc) and *n*-hexane were used after simple distillation with a boiling chip.

Animals

All laboratory animals were obtained from Orient Bio, Inc. (Gyeonggi-do, South Korea). All procedures were pre-approved by the Institutional Animal Care and Use Committee at the Asan Medical Center and at the Korea Institute for Science and Technology and were conducted in accordance with the Guide for Care and Use of Laboratory Animals (National Institute of Health, USA).

Synthesis of KKC080106 and structural analysis

4,6-Dichloro-2-(methylthio)pyrimidine-5-carbaldehyde (Compound 2): A volume of 43.5 ml of phosphoryl chloride (0.37 mol, 5.8 equi.) was placed into a 250 ml 3-neck flask. The reaction temperature was lowered to 0 ˚C, and 14 ml dimethylformamide (0.18 mol, 2.8 equi.) was added drop by drop, after which the reaction was allowed to continue at room temperature for 1 h. 2-(Methylthio)pyrimidine-4,6-diol (Compound 1; 10 g, 63.2 mmol) was then added into the reactor and heated for 24 h at 100 ˚C. The reaction progress was monitored by thin layer chromatography (using *n*-hexane/EtOAc: 10/1); the R_f value of the product (ultraviolet-active) was 0.42. After the reaction was completed, the mixture was poured into ice water and kept for 6 h to allow the yellowish solid to settle down. After filtration, the filtrate was neutralized with $NaHCO_3$,

and the product was extracted with EtOAc, dried over anhydrous $MgSO_4$, and evaporated to obtain a solid crude product, which was then dissolved in 5 ml of EtOAc and 300 ml of *n*-hexane by continuous shaking. A yellowish solid was allowed to form overnight at 4 °C, isolated by filtration using only *n*-hexane, and dried under high vacuum (0.875 g). Yield: 62 %; ^{1}H NMR (400 MHz, DMSO-d_6) δ 1.54 (d, J = 6.5 Hz, 3H), 2.42 (s, 3H), 5.42 (s, 3H), 7.19 -7.41 (m, 8H), 7.41 (d, J = 7.1 Hz, 2H), 8.15 (s, 1H), 8.74 (d, J = 7.1 Hz, 1H); ^{13}C NMR (100 MHz, DMSO-d_6 δ 14.0, 22.8, 49.6, 50.1, 98.5, 126.5, 127.2, 128.0, 128.8, 128.9, 132.8, 137.7, 145.0, 154.0, 154.9, 168.9.

1-Benzyl-4-chloro-6-(methylthio)-1H-pyrazolo[3,4-*d*]pyrimidine (Compound 3): Compound 2 (1 g, 4.5 mmol) was dissolved in 32 ml of a solvent mixture (THF/H_2O: 3/1), after which 1.5 equivalents of Hunig base was added drop by drop followed by benzyl-N_2H_3 H_2O (0.76 g, 1.2 equiv); the reaction mixture was then stirred at room temperature for 3 h. The reaction progress was monitored by thin layer chromatography (using *n*-hexane/EtOAc: 1/1), the R_f value of the product (ultraviolet-active) was 0.11. After the reaction was completed, the mixture was poured into ice water and kept for 2 h to allow the yellowish solid to precipitate. The product was then filtered, and the precipitation procedure was repeated two more times. The pure product (a yellow solid) was isolated by filtration using only hexanes and dried under high vacuum (1.01 g). Yield: 77.2 %; a pale-yellow solid; ^{1}H NMR (400 MHz, $CDCl_3$) δ 2.62 (s, 3H), 5.57 (s, 2H), 7.25-7.36 (m, 5H), 8.01 (s, 1H).

1-Benzyl-6-(methylthio)-*N*-(1-phenylethyl)-1*H*-pyrazolo[3,4-*d*]pyrimidine-4-amine (Compound 4) - KKC080106: Compound 3 (300 mg, 1 mmol) was dissolved in 20 ml

1,4-dioxane and reacted with phenylethylamine (133 mg, 1.1 equi.) under reflux condition for 8 h. After completion, the reaction mixture was diluted with water, and the product was extracted with EtOAc, dried over anhydrous $MgSO_4$, and evaporated to obtain a brown solid (0.323 g). Yield: 90.2 %; ^{1}H NMR (400 MHz, DMSO-d_6) δ 1.54 (d, J = 7.0 Hz, 3H), 2.42 (s, 3H), 5.42-5.45 (m, 3H), 7.20-7.34 (m, 8H), 7.41 (d, J = 7.2 Hz, 2H), 8.17 (s, 1H), 8.74 (d, J = 7.6 Hz, 1H); ^{13}C NMR (100 MHz, DMSO-d_6) δ 13.5, 22.3, 49.1, 49.6, 98.0, 126.0, 126.7, 127.4, 127.5, 128.2, 128.4, 132.3, 137.2, 144.5, 153.5, 154.4, 168.4.

Cell cultures

The mouse microglial BV-2 cells (Blasi et al., 1990) were grown in Dulbecco's modified Eagle medium with 10% FBS. The mouse dopaminergic neuronal CATH.a cells (Suri et al., 1993) were cultured in RPMI culture medium 1640 containing 8% horse serum and 4% FBS. Cells were maintained in the presence of 100 IU/l penicillin and 10 µg/ml streptomycin at 37 °C in a 5% CO_2 humidified atmosphere. For treatment, KKC080106 was prepared as a 100 mM stock solution dissolved in DMSO and diluted with the respective culture media. The final concentration of DMSO in the cell culture did not exceed 0.02% for both KKC080106-treated and control cells.

NO assay

According to Son et al. (2014), 200 µl aliquots of the culture medium of BV-2 cells were mixed with 100 µl of the Griess reagent (1% sulfanilamide and 0.1% naphthylethylenediamine dihydrochloride in 2.5% H_3PO_4) in a 96 well microtiter plate. The absorbance at 540 nm was obtained using a plate reader. The nitrite concentration

was determined using the standard curve of sodium nitrite that was generated every time.

HO-1 induction assay by ELISA

We added 50 μl of lysis solution (150 mM NaCl, 50 mM Tris-HCl, pH 8.0, and 1% Nonidet-P40) to a BV-2 cell pellet, and the sample was incubated on ice for 20 min. After centrifugation for 15 min (3,000 ×*g*), the supernatant was diluted 10 times with 50 mM Tris-HCl buffer (pH 8.0). Sandwich ELISA for HO-1 was carried out using capture and detection HO-1 antibodies based on the method of Woo et al. (2014).

RT-PCR

In order to assess changes in mRNA levels, we used reverse transcription (RT) PCR as the results correspond with those of real-time PCR in this experimental system (Lee et al., 2015a). RT reactions were performed using 5 μg of total RNA and the First Strand cDNA Synthesis kit following the manufacturer's instructions.

The following primers were used: HO-1 (forward, 5'-AGCAGGACATGGCCTCT-3'; reverse, 5'-TCTGTCAGCATCACCTGCAG-3'), NQO1 (forward, 5'-CCATCCTAAACAGCGATCA-3'; reverse, 5'-TAGCTTTGATCTGGTTGTC-3'), GCLC (forward, 5'-ATGACTGTTGCCAGTGGATGAGA-3'; reverse, 5'-ACACGCCATCCTAAACAGCGATCA-3'), GCLM (forward, 5'-AGCTGGACTCTGTGATCATGGCTT-3'; reverse, 5'-CAAAGGCAGTCAAATCTGGTGGCA-3'), IL-1β (forward, 5'-ATGGCAACTGTTCCTGAACTCACCT-3'; reverse, 5'-CAGGACAGGTATAGATTCTTTCCTTT-3'), TNF-α (forward, 5'-

CAGACCCTCACACTCAGATCATCTT-3'; reverse, 5'-CAGAGCAATGACTCCAAAGTAGACCT-3'), inducible NO synthase (iNOS) (forward, 5'-ATGTCCGAAGCAAACATCAC-3'; reverse, 5'-TAATGTCCAGGAAGTAGGTG-3'), cyclooxygenase-2 (COX-2) (forward, 5'-CAGCAAATCCTTGCTGTTCC-3'; reverse, 5'-TGGGCAAAGAATGCAAACATC-3'), and glyceraldehyde 3-phosphate dehydrogenase (GAPDH) (forward, 5'-CACCACCATGGAGAAGGCTGG-3'; reverse, 5'-TTGTCATGGATGACCTTGGCCAGG-3'). Densitometric analyses were performed using ImageJ program (Schindelin et al., 2012). The data were normalized against the densitometric value of GAPDH.

Cell viability test

Cell viability was assessed by measuring the intracellular ATP level using the CellTiter-Glo Luminescent Cell Viability Assay kit according to the method of Woo et al. (2014). The degree of cell death was assessed by determining the activity of lactate dehydrogenase (LDH) released into the culture medium based on the method of Cho et al. (2009). For trypan blue exclusion assay, cells were exposed to 0.1% trypan blue dye, incubated for 2 min, and counted on a hemocytometer. The percentage of viable cells was calculated as the number of unstained cells divided by the total number of cells. The cells were also observed with differential interference contrast microscopy to identify morphological changes.

Western blot analysis

After nuclear fractions and cell lysates were obtained, equal amounts (30 μg) of

protein were subjected to western blot analysis according to the method of Woo et al. (2014) and Lee et al. (2018a). The primary antibodies used were: Nrf2 (1:2,000), HO-1 (1:200), GCLC (1:3,000), GCLM (1:200), NQO1 (1:1,000), p-IKK (1:1,000), IKK (1:200), p-ERK (1:1,000), ERK (1:1,000), p-p38 (1:1,000), p38 (1:1,000), p-JNK (1:1,000), JNK (1:1,000), lamin B (1:200), HSP90 (1:1000), and β-actin (1:60,000). After incubating with horseradish peroxidase-conjugated secondary antibodies, protein bands were visualized using a chemiluminescence substrate and quantified by densitometry.

Measurement of TNF-α and IL-1β levels

The culture medium and cell lysate of BV-2 cells were subjected to TNF-α and IL-1β measurements using the respective ELISA kits (Son et al., 2016). The concentrations of TNF-α and IL-1β were calculated from the corresponding standard curves.

Surface plasmon resonance analysis

The Biacore T100 instrument (GE Healthcare, Uppsala, Sweden) was used to perform surface plasmon resonance analysis at 25 °C according to the method of Lee et al. (2018b). Anti-His antibody was first immobilized onto CM5 chips using the amine coupling kit and the His capture kit (GE Healthcare). After deactivation of the CM5 chip surface, purified His-tagged Keap1 (100 μg/ml) was injected for 150 s over the immobilized anti-His antibody. To prepare KKC080106 solutions, 0.5–10 mM stock solutions were first prepared in 10 % DMSO and then diluted 10 times with HBS-EP$^+$ (GE Healthcare). KKC080106 was then injected at a flow rate of 30 μl/min for 180 s to

allow binding with Keap1, followed by dissociation for 300 s. Upon completion of each cycle, the sensor chip was regenerated by injecting 10 mM glycine-HCl (pH 1.5) at 30 μl/min for 60 s. The sensograms were obtained and analyzed using the BIAevaluation software (GE Healthcare). Prior to the calculations, we corrected the binding data for non-specific interactions by subtracting the reference surface value (running buffer only) from the reaction surface value.

Proteasomal enzyme activity assays

Purified human 26S proteasome (0.1 μg) was incubated with KKC080106 and 40 μM (final concentration) of the fluorogenic peptide substrates Suc-Leu-Leu-Val-Tyr-AMC, Boc-Leu-Arg-Arg-AMC, or Z-Leu-Leu-Glu-AMC in an 100 μl assay buffer (50 mM Tris-HCl, pH 7.5). After 2 h, the released fluorogenic AMC was measured by a fluorometric plate reader (SpectraMax Gemini XPS; Molecular Devices, Menlo Park, CA, USA) at 368 nm excitation and 467 nm emission. The activity of each protease was determined by measuring the increase in fluorescence intensity; the data are expressed as the percentage respective to the untreated control.

Stability against plasma enzymes

After preincubation for 5 min at 37 °C, 297 μl of the plasma enzyme preparation (from human, dog, rat, and mouse) was mixed with 3 μl of 100 μM KKC080106 and incubated further. At 0, 30, 60, 120 and 360 min, 50 μl of the reaction mixture was transferred into a tube containing 100 μl acetonitrile and centrifuged for 10 min at 10,000 $\times g$ at room temperature. The supernatant was then subjected to the LC-MS/MS analysis (Triple Quad 5500, Applied Biosystems, USA) in order to determine

the amount of the remaining KKC080106 using a standard curve of 5-1,000 ng/ml of KKC080106.

Pharmacokinetic profiles in mice and rats

We used male C57BL/6 mice (7–9 weeks old) and male Sprague-Dawley rats (8 weeks old). For intravenous injection, KKC080106 was dissolved in a solution containing 2% DMSO and 20% 2-hydroxypropyl-β-cyclodextrin to yield a final concentration of 1 mg/ml (pH 7.0). For oral administration by gavage, KKC080106 was dissolved in a solution containing 10% N-methyl-2-pyrrolidone and 20% Tween 80 to yield a final concentration of 3 mg/ml (pH 7.0). The control blood sample was obtained prior to the administration. The blood was collected from the jugular vein into a heparinized tube and centrifuged at 11,700 ×g for 15 min to obtain the plasma; after which, 80 µl of acetonitrile (containing internal standard) was mixed with 20 µl of the plasma. The sample was then centrifuged at 16,000 ×g for 5 min to obtain the supernatant. Whole brains were homogenized in four volumes of ice-cold deionized water using a tissue homogenizer (12,000 rpm, 30 s), after which the homogenates were processed as described above. The samples were then subjected to the LC-MS/MS analysis. The pharmacokinetic parameters were determined by non-compartmental analysis using the Phoenix WinNolin software version 6.4 (Pharsight, USA).

***In vivo* single dose toxicity test**

KKC080106 was orally administered in male Sprague-Dawley rats (8 weeks old) by gavage at doses of 0, 500, 1,000, and 2,000 mg/kg body weight according to the

OECD guidelines in which the upper limit dosage is 2,000 mg/kg at a single dose (OECD, 2008). Toxicity was assessed based on mortality and general signs and symptoms of toxicity (changes in skin/fur, eyes and mucous membranes, motor activity, and behavior pattern; presence of tremors, convulsions, salivation, diarrhea, lethargy, sleep, and coma) observed for 14 days based on OECD guidelines (OECD, 2008).

In vitro hERG channel assay

CHO-K1 Tet-On hERG cells were incubated in MEM with 10% FBS. hERG channel expression was induced by exposure to doxycycline (1 µg/ml) for 20 h prior to use. The composition of solutions used to measure the hERG channel activity was as follows: external cellular solution: 140 mM NaCl, 2 mM $CaCl_2$, 4 mM KCl, 1 mM $MgCl_2$, 5 mM D-glucose, and 10 mM HEPES (pH 7.4); internal cellular solution: 50 mM KCl, 10 mM NaCl, 60 mM KF, 2 mM $MgCl_2$, 10 mM HEPES (pH 7.2), and 20 mM EGTA; seal enhancer: 80 mM NaCl, 35 mM $CaCl_2$, 3 mM KCl, 10 mM $MgCl_2$, and 10 mM HEPES (pH 7.4). We used the auto patch clamp machine NPC©-16 Patchliner (Nanion Technologies, Germany) and the whole-cell patch clamp technique. Channel current was recorded with an EPC10 amplifier (HEKA, Germany). Cell suspension and patch solutions were automatically divided into the chip (NPC-16 Chip, Nanion Technologies, Germany).

Animals treated with MPTP and KKC080106

Male C57BL/6 mice (23–25 g) were kept in a humidity- and temperature-controlled room with a 12 h light-dark cycle; food and water were available *ad libitum*.

The animals were randomized into three groups (10 animals/group): control, MPTP, and MPTP+KKC080106. KKC080106 was suspended in 10% N-methyl-2-pyrrolidone and 20% Tween 80 (pH 7.0) and administered orally at a dose of 30 mg/kg three times daily. Meanwhile, the control and MPTP groups received the vehicle only. One hour after the second KKC080106 administration, animals in the MPTP and in MPTP+KKC080106 groups were injected intraperitoneally MPTP dissolved in saline four times every 2 h at a dose of 20 mg/kg body weight, while animals in the control group were injected saline only. Each animal was kept in an individually-ventilated cage at the Asan Institute for Life Science. Behavior tests and euthanasia were carried out in a separate room in order to minimize the emotional distress experienced by the remaining live animals.

Immunohistochemistry

Based on the method of Son et al. (2012), the animals were deeply anesthetized seven days after the MPTP injection and subjected to transcardial paraformaldehyde perfusion. The brains were removed, postfixed in 4% paraformaldehyde, and cryoprotected in 30% sucrose. Samples were then cut into 20 μm sections with a sliding microtome (Model HM 450, Thermo Fisher Scientific), delineating the nigral and striatal regions according to the Mouse Brain Atlas (Franklin and Paxinos, 1997). For TH immunostaining, a total of five sections (every fourth section, 80 μm apart) of the substantia nigra (SN) and striatum were taken from each animal; we ensured that the sections from each brain represented the same anatomical region. For Iba-1 immunostaining, an additional five sections of the SN, each posteriorly adjacent to those taken for the TH immunostaining, were obtained. The sections were exposed to the corresponding antibodies, TH (1:1,000) or Iba-1 (1:200), and processed using the

Vectastain ABC kit and biotinylated secondary antibodies. The sections were then incubated in 0.05% 3,3'-diaminobenzidine and 0.003% H_2O_2 in order to visualize the immunoreactivities. The TH-immunopositive neurons of SN sections were counted using the Mousotron 3.8.3 Black Sun Software (Turnhout, Belgium), while the TH-immunopositive fibers in the striatum and the Iba-1-immunopositive microglial cells of SN sections were quantitated by densitometry using Image Gauge 4.0 software (Fujifilm, Tokyo, Japan). The final immunodensity values were obtained after subtracting the background density from regions lacking immunoreactivity.

Hindlimb test

The mice were subjected to the hindlimb test six days after being injected with MPTP (Lee et al., 2016). The animals were suspended by the tail, and their hindlimb posture was scored on a scale of 0-4. A score of 4 was given when both hindlimbs were splayed outward with no clasping of the toes, considered a typical behavior. Whenever there was an incomplete splay of a hindlimb (retracted toward the abdomen), a score of 1 was deducted. Whenever the toes were curled (clasping) on either hindlimbs, another score of 1 was deducted.

Rotarod test

According to Son et al. (2017), on the three days prior to the MPTP injection, mice were trained on a rotarod (Ugo Basile Biological Research, Varese, Italy) with a rotating speed of 20 rpm for 150 s twice a day. On the sixth day post-injection, we recorded how long each mouse remained on the rotarod with a rotating speed of 30 rpm.

A total of three trials were taken; the animals were allowed to rest for 60 min between trials.

Vertical grid test

According to Kim et al. (2010b), on the three days prior to the MPTP injection, the mice were trained to scale, turn around, and descend on the vertical apparatus twice a day. On the sixth day post-injection, the animals were tested on the same vertical grid and videotaped. The videos were analyzed in order to determine the time taken for each mouse to turn around and climb down; we also recorded the total time taken in the vertical apparatus and the number of successful hindlimb steps.

Horizontal grid test

A horizontal grid test was performed based on Kim et al. (2010b). Briefly, the animals were allowed to familiarize with the horizontal grid apparatus twice a day on the three days prior to the MPTP injection. On the sixth day post-MPTP injection, their motor activities on the apparatus were videotaped and later analyzed to determine the total number of successful steps and the distance traveled (sum of steps).

Data analyses

Statistical tests were carried out using PRISM software (San Diego, CA, USA). A value of $p<0.05$ was considered statistically significant. Comparisons between groups were analyzed by one-way analysis of variance; for comparisons between three or more groups, post Dunnett's multiple comparison tests were also carried out. At least three independent experiments were performed for *in vitro* studies and the data are expressed

as mean ± SEM.

Results

Construction and screening of a pyrazolo [3,4-*d*] pyrimidine library and discovery of KKC080106

We have designed and generated a library consisting of 241 pyrazolo [3,4-*d*] pyrimidines in which several functional groups have been substituted (Fig. 1A). Based on the findings that Nrf2 activation increases HO-1 expression and decreases NO production, a cell-based assay system was established to measure HO-1 and NO in order to indirectly evaluate Nrf2 activity and successfully obtain Nrf2-activating compounds (Lee et al., 2015a; 2015b). The same approach was used in the present study to screen the pyrazolo [3,4-*d*] pyrimidine library. Such screening first generated data on the effects of each compound on NO production in LPS-challenged BV-2 microglia and on HO-1 expression in unchallenged cells. After excluding compounds that were cytotoxic, predicted to be chemically unstable, or had low solubility in aqueous solutions, we selected those that decreased NO generation to at least 80%. For each of these 78 pyrazolo [3,4-*d*] pyrimidines, the degree of NO downregulation was plotted against the degree of HO-1 induction, where KKC080106, (R)-1-benzyl-6-(methylthio)-*N*-(1-phenylethyl)-1*H*-pyrazolo[3,4-*d*]pyrimidine-4-amine, was finally selected for its excellent NO-production inhibition and HO-1 induction activities (Fig. 1B). The chemical structure of KKC080106 and its synthesis scheme are shown in Fig. 1D.

KKC080106 can act stereospecifically and is non-electrophilic/non-cytotoxic

For a chiral compound to be used as a drug, obtaining a single enantiomer with stereospecificity is highly advantageous. Since KKC080106 has chirality, we asked whether it might act stereospecifically by testing its S-enantiomer KKC080227. The

results showed that KKC080227 has no HO-1 upregulating or NO-downregulating activities (Fig. 1B, marked in blue), indicating that the R-enantiomer KKC080106 can stereospecifically exert its effects. The chemical structure of KKC080106 also revealed that it contains no electrophilic moiety. We examined whether the absence of electrophilicity might counteract the cytotoxicity that had been observed with the electrophilic Nrf2 activators. KKC080106 had no effect on cell viability in the concentration range tested (Fig. 1C). On the other hand, the electrophilic Nrf2 activator, CDDO-Me, was highly cytotoxic, leaving almost no viable cells at 1 μM. Although less cytotoxic, sulforaphane began to affect cell viability at ~5 μM. The lack of cytotoxicity of KKC080106 was further confirmed by the LDH release assay and trypan blue exclusion assay, which showed no change in cell viability with increasing concentrations of the compound (Fig. 1D). In addition, morphological analysis revealed no apparent signs of cell damage (Fig. 1D).

KKC080106 activates Nrf2 signaling

Given Nrf2 is normally bound to its inhibitor protein (Keap1) and then degraded, an increase in Nrf2 levels suggest its release from Keap1. Western blot analysis on CATH.a dopaminergic neuronal cells showed that, after exposure to KKC080106, Nrf2 levels significantly increased in a dose-dependent manner (Fig. 2A).

Since Nrf2 is degraded by the ubiquitin-proteasomal system, the increase in Nrf2, apparently caused by KKC080106, might actually be due to an effect on the ubiquitin-proteasomal system. Thus, we tested the proteasomal activities in the presence of the compound. Our results showed that the chymotrypsin-like, trypsin-like, and caspase-like activities of the proteasome were not altered by KKC080106, whereas the

known proteasomal inhibitor MG-132 reduced the activities of all three proteases (Fig. 2B), indicating that the increase in Nrf2 is not related to the proteasomal activities.

The significant increase in Nrf2 levels might be due to KKC080106 acting on Keap1 protein itself. To test this, we performed a surface plasmon resonance analysis. Our results showed that KKC080106 indeed caused changes in the surface plasmon resonance of Keap1, suggesting that there is direct binding between the two molecules (Fig. 2C). The affinity of such binding appeared to be high as the dissociation constant (Kd) was calculated to be 5.84×10^{-10} M.

Having observed that KKC080106 can bind to Keap1, we investigated whether this actually leads to the translocation of Nrf2 into the nucleus and found that KKC080106 caused the accumulation of nuclear Nrf2 in a dose-dependent manner (Fig. 2D).

Induction of Nrf2 target genes would be another indicator of Nrf2 activation. Given that the antioxidative/neuroprotective enzyme genes NQO1, HO-1, GCLC, and GCLM are targets of Nrf2, we investigated whether KKC080106 increases the expression levels of these genes. Our results showed that all four enzyme genes increased dramatically with KKC080106 in CATH.a cells (Fig. 2E and F). Therefore, the concomitant expression of known Nrf2 target genes provides further evidence that KKC080106 causes Nrf2 activation.

Anti-inflammatory effects of KKC080106

In BV-2 microglial cells that had been activated with LPS, KKC080106 was able to suppress the increase in the levels of inflammatory mediators (Fig. 3). NO production decreased in a dose-dependent manner, with 30 μM of KKC080106 causing

a decrease of 73% (Fig. 3A). Moreover, 20 μM of KKC080106 abolished the LPS-induced increase in iNOS mRNA levels (Fig. 3D, $p>0.05$). IL-1β was also dramatically downregulated, with 20 μM of KKC080106 almost completely suppressing the LPS effect at both the protein and mRNA levels (Fig. 3B and D, $p>0.05$). The effect on TNF-α was also significant, although to a lesser extent (Fig. 3C and D). In addition, the expression of COX-2 (a proinflammatory enzyme) was effectively suppressed by KKC080106 (decreased by 91% with 20 μM; Fig. 3D). These results indicate that KKC080106 is able to suppress the production of pro-inflammatory molecules.

Several kinases are known to mediate inflammatory signaling, such as IKK and the MAP kinases ERK, p38, and JNK (Dong et al., 2002; li, 2006), and Nrf2 and its target product HO-1 are believed to interfere with this signaling (Li et al., 2008; Morse et al., 2003; Silva et al., 2006). In the LPS-activated BV-2 cells, KKC080106 inhibited IKK activation, demonstrated by the dose-dependent decrease in the phosphorylated form (Fig. 3E). Additionally, KKC080106 also affected the MAPK signaling pathways (Fig. 3F). While LPS treatment caused an increase in the levels of phosphorylated JNK, this was suppressed in the presence of KKC080106. The phosphorylated forms of p38 and ERK were also similarly reduced. Therefore, our results suggest that KKC080106 suppresses the activation of kinases involved in inflammatory signaling pathways.

Safety profile of KKC080106

Having confirmed the efficiency of KKC080106 *in vitro*, we evaluated the compound's utility as a drug prior to proceeding to *in vivo* studies. As drugs should have no adverse effects *in vivo,* KKC080106 was first subjected to a single-dose toxicity test. We administered KKC080106 at 500, 1,000, and 2,000 mg/kg body weight by oral

gavage and observed the animals for 14 days. We observed no mortality, and the animals showed none of the general signs of toxicity (Table 1). Based on these observations, KKC080106 was predicted to be safe *in vivo*, with its median lethal dose value greater than 2,000 mg/kg.

Given that blocking the hERG potassium channel activity causes serious cardiovascular problems (Recanatini et al., 2005), it is crucial to certify that new candidate drugs will not inhibit the potassium channel activity. We therefore evaluated the effect of KKC080106 on the hERG channel by performing a whole cell patch clamp assay. The resulting IC_{50} value was determined to be 10.3 μM. As drug candidates with IC_{50} values greater than 10 μM are considered to have a minimum interaction with the hERG channel (Dumotier et al., 2008), it is unlikely that KKC080106 could cause serious cardiovascular problems.

Stability against plasma enzymes

To be considered an effective drug, it is important that the compound administered into the body is not degraded by hydrolytic enzymes in the plasma. We therefore investigated the stability of KKC080106 against plasma enzymes from four different species: human, dog, rat, and mouse. Only a small fraction of the compound was degraded by the enzymes of humans, dogs, and mice, with large portions of the compound (75–86%) remaining after 6 h (Table 2). KKC080106 was found to be relatively less stable against rat enzymes, but the value was still within the acceptable range of stability (38% remaining after 6 h).

Bioavailability and brain penetration

Whether or not a compound can be used as a drug also depends on its pharmacokinetic properties. Moreover, the ability to cross the blood brain barrier is essential for drugs targeting the central nervous system. We performed pharmacokinetic analysis on mice and rats that had been dosed intravenously or orally with KKC080106. In mice, the bioavailability reached a relatively high value of 57%, and the brain/plasma ratio was 26% and 15% after intravenous and oral administrations, respectively (Table 3). The bioavailability in rats was also within the acceptable range (34%) and the brain penetration was evident with the brain/plasma ratio reaching 43% and 37% after intravenous and oral administrations, respectively (Table 4).

KKC080106 protected nigral dopaminergic neurons

Having established that KKC080106 enters the brain and is expected to have little adverse effects, we evaluated the efficiency of KKC080106 *in vivo* by assessing its neuroprotective effect on nigral neurons using mice administered MPTP, the widely used toxin that causes selective degeneration of the nigrostriatal dopaminergic system mimicking PD (Dauer and Przedborski, 2003). Immunostaining against TH, a dopaminergic marker revealed that while MPTP caused a significant decrease in TH-positive neurons (Fig. 4A - left panel), the orally administered KKC080106 provided significant protection. Quantitative analysis revealed that the number of TH-positive neurons in the MPTP group was only 26% of the vehicle-treated control, but much higher in the MPTP+KKC080106 group (87%, Fig. 4B). In the striatum, the brain region to which the nigral dopaminergic neurons project their fibers, the TH-immunoreactive fibers nearly disappeared among MPTP-treated animals (Fig. 4A - right panel and Fig. 4C; 9% of vehicle-treated control), but this decrease was largely

attenuated by KKC080106 (68%).

KKC080106 suppressed microglial activation

MPTP treatment is known to cause microglial activation in the nigrostriatal region, which further aggravates the neurodegeneration (Kurkowska-Jastrzebska et al., 1999). Using MPTP-treated mice, we evaluated the anti-inflammatory efficiency of KKC080106 *in vivo*. Immunocytochemistry of the nigral brain sections compared against the microglial marker Iba-1 (Sierra et al., 2007) revealed that the number of activated microglia increased in MPTP-treated animals (194% compared to the vehicle-treated control; Fig. 4D and E). On the other hand, among MPTP+KKC080106-treated animals, there were no apparent differences in morphology or number of Iba-1-immunopositive cells when compared to the vehicle-treated control animals (112%, $p>0.05$).

KKC080106 improved motor performance

We examined whether KKC080106 could alleviate the motor deficits caused by dopaminergic degeneration using several behavioral tests that have previously provided reliable measures of PD-related motor activity in MPTP-treated mice (Kim et al., 2010; Lee et al., 2016). In the hindlimb test, while the MPTP group scored only 53% relative to the score obtained by the vehicle control group, the MPTP+KKC080106 group scored 82% (Fig. 5A). Animals treated with MPTP were able to hold on to the rotating rod for only 62 s, while animals from the control managed for 147 s; however, animals from the MPTP+KKC080106 group were able to hold on to the rod for 181 s (Fig. 5B). Regarding the horizontal grid test, which evaluates neuromuscular strength and

coordination, MPTP-treated animals made shorter strides, reducing the sum of step distance by 74% in relation to the control group, and showed less successful steps, but animals treated with KKC080106 reversed these phenomena (Fig. 5C and D). In the vertical grid test, which measures bradykinesia and motor deficits, MPTP-treated animals took much longer to climb down and turn around on the grid (155% and 350%, respectively) in relation to the control group, resulting in a higher total time spent on the apparatus (Fig. 5E-G). However, MPTP+KKC080106-treated animals were able to overcome these deficits (95%, 110%, and 100%, respectively; $p>0.05$) (Fig. 5E-G). Furthermore, while the number of successful hindlimb steps made by the MPTP-treated animals was only 73% in relation to the control, no such decrease was observed in the MPTP+KKC080106 group (Fig. 5H). Overall, the behavioral parameters tested revealed that KKC080106 can effectively alleviate the motor deficits associated with dopaminergic degeneration.

Discussion

We report the screening of a novel pyrazolo [3,4-*d*] pyrimidine library and the discovery of KKC080106, which binds to Keap1 and activates Nrf2 signaling. As a result, KKC080106 induces the expression of Nrf2 target antioxidative/anti-inflammatory enzyme genes while suppressing the expression of pro-inflammatory genes. KKC080106 was found to be safe and to show a favorable pharmacokinetics profile, including the ability to enter the brain. It was highly effective *in vivo* after oral administration: it protected nigral neurons, suppressed microglial activation, and alleviated the motor deficits in MPTP-treated mice (model of PD).

MPTP, once converted to MPP+ and taken into dopaminergic neurons, causes cell damage by inhibiting the mitochondrial electron transfer and exerting oxidative stress (Drechsel and Patel, 2008). The dead/damaged neurons can trigger activation of nearby microglia, whose production/release of NO and cytotoxic cytokines leads to further neuron death, creating a vicious cycle of neuroinflammation (Block et al., 2007). In this context, the neuroprotective effect of KKC080106 *in vivo* appears to involve both anti-oxidative and anti-inflammatory mechanisms, both of which are consequences of Nrf2 activation. In other words, KKC080106 leads to activation of Nrf2 and induction of the antioxidative enzymes NQO1, HO-1, and GCL, all of which are known to protect dopaminergic neurons against MPP+ (Ahuja et al., 2016; Guo et al., 2019). Furthermore, KKC080106 can directly exert anti-inflammatory effects on the activated microglia themselves by lowering the production/release of NO and IL-1β/TNF-α. Therefore, any activated microglia would no longer cause deleterious effects on nearby neurons. Because MPTP is first metabolized to MPP+ by the glial monoamine oxidase B before entering the dopaminergic neurons via dopamine transporters, it is possible

that KKC080106 may affect these proteins, where the neuroprotection should be partially mediated by such action.

Keap1 is a cytosolic protein that binds with Nrf2 and promotes its degradation, thereby causing a negative regulation of the genes involved in antioxidative and anti-inflammatory responses. Keap1 contains critical cysteine thiols that react with electrophiles (Deshmukh et al., 2017), whose covalent modification leads to liberation of Nrf2 (Saito et al., 2015). To minimize the side effects associated with electrophilic Nrf2 activators, researchers have investigated non-electrophilic peptides that interfere with Keap1-Nrf2 binding (Gazaryan and Thomas, 2016; Steel et al., 2018; Tu et al., 2015). The relatively large size of peptides, however, is a restraint as many are unable to cross the blood-brain barrier. We found a small molecule, KKC080106, that is able to enter the brain, contains no electrophilic moiety, yet still binds to Keap1 and activates the Nrf2 signaling, which suggests that it may interact with Keap1 in a non-covalent manner. Such interaction can occur via attraction between molecules that have flat ring structures; these pi-pi stacking interactions contribute to high affinity binding, which is essential for protein-ligand recognition (Zhao et al., 2015). KKC080106 has two aromatic rings, which are substituted at the N-position of the pyrazole ring and the pyrimidine site. In Keap1, the aromatic amino acids Phe577, Tyr334, and Tyr 572 are present in the kelch domain of Keap1 (i.e., the Nrf2-binding region), and they are the residues commonly addressed by small-molecule inhibitors (Schmoll et al., 2017). Therefore, it is possible to speculate that the two aromatic rings in KKC080106 and the aromatic rings of the amino acids on Keap1 form the pi-pi stacking interactions, resulting in the high affinity binding observed between KKC080106 and Keap1.

KKC080106 was found to possess many advantages as a potential drug. First, as it has no electrophilic group, it possesses relatively little safety issues. Indeed, the *in vitro* tests showed no apparent cytotoxicity or hERG inhibition, and the *in vivo* acute toxicity test revealed no lethality at a dose as high as 2,000 mg/kg. Second, KKC080106 could reach the brain; it was stable against degradation by the plasma enzymes and showed good bioavailability and brain-to-plasma ratio. Third, KKC080106 is effective after oral gavage, which is the preferred and the most convenient route of drug administration. Fourth, KKC080106 acts in a stereospecific manner as the stereo isomer of the pyrimidine site has no activity. Given proteins associate with binding partners in a stereospecific manner and an enantiomeric mixture is undesirable as a drug (Brooks et al., 2011; Nguyen et al., 2006), the successful identification and synthesis of the effective enantiomer is a great advantage.

Conclusions

Our novel pyrazolo [3,4-*d*] pyrimidine, KKC080106, binds to Keap1 with high affinity and activates Nrf2 (and the subsequent signaling pathway), inducing the expression of antioxidative enzymes known to exert neuroprotective effects. KKC080106 also suppresses proinflammatory signaling pathways and the production of proinflammatory molecules. *In vivo*, KKC080106 was able to protect nigral dopaminergic neurons, reduce microglial activation, and alleviate the associated motor deficits. To our knowledge, KKC080106 is the first pyrazolo [3,4-*d*] pyrimidine that has demonstrated such activity. Additionally, KKC080106 acts most likely without electrophilic/covalent interactions, minimizing the risk of toxicity. As a potential drug for the central nervous system, KKC080106 showed a good safety and pharmacokinetic

profile. Overall, KKC080106 has therapeutic potential for neurodegenerative disorders such as PD.

Acknowledgements

Funding: This research was supported by the National Research Foundation of Korea (grant numbers: 2009-0081674,5 and 2018R1A6A3A01010334), South Korea.

Conflict of interest

There are no conflicts of interest to disclose.

References

Abed, D.A., Goldstein, M., Albanyan, H., Jin, H., Hu, L., 2015. Discovery of direct inhibitors of Keap1-Nrf2 protein-protein interaction as potential therapeutic and preventive agents. Acta Pharm. Sin. B. 5, 285-299.

Ahmed, S.M., Luo, L., Namani, A., Wang, X.J., Tang, X., 2017. Nrf2 signaling pathway: pivotal roles in inflammation. Biochim. Biophys. Acta. Mol. Basis Dis. 1863, 585-597.

Ahuja, M., Ammal Kaidery, N., Yang, L., Calingasan, N., Smirnova, N., Gaisin, A., Gaisina, I.N., Gazaryan, I., Hushpulian, D.M., Kaddour-Djebbar, I., Bollag, W.B., Morgan, J.C., Ratan, R.R., Starkov, A.A., Beal, M.F., Thomas, B., 2016. Distinct Nrf2 signaling mechanisms of fumaric acid esters and their role in neuroprotection against 1-methyl-4-phenyl-1,2,3,6-tetrahydropyridine-induced experimental Parkinson's-like disease. J. Neurosci. 36, 6332-6351.

Baier, S.R., Zbasnik, R., Schlegel, V., Zempleni, J., 2014. Off-target effects of sulforaphane include the derepression of long terminal repeats through histone acetylation events. J. Nutr. Biochem. 25, 665-668.

Blasi, E., Barluzzi, R., Bocchini, V., Mazzolla, R., Bistoni, F., 1990. Immortalization of murine microglial cells by a v-raf/v-myc carrying retrovirus. J. Neuroimmunol. 27, 229-237.

Block, M.L., Zecca, L., Hong, J.S., 2007. Microglia-mediated neurotoxicity: uncovering the molecular mechanisms. Nat. Rev. Neurosci. 8, 57-69.

Brooks, W.H., Guida, W.C., Daniel, K.G., 2011. The significance of chirality in drug design and development. Curr. Top. Med. Chem. 11, 760-770.

Burton, N.C., Kensler, T.W., Guilarte, T.R., 2006. In vivo modulation of the Parkinsonian phenotype by Nrf2. Neurotoxicology. 27, 1094-1100.

Chauhan, M., Kumar, R., 2013. Medicinal attributes of pyrazolo[3,4-d]pyrimidines: a review. Bioorg. Med. Chem. 21, 5657-5668.

Chen, P.C., Vargas, M.R., Pani, A.K., Smeyne, R.J., Johnson, D.A., Kan, Y.W., Johnson, J.A., 2009. Nrf2-mediated neuroprotection in the MPTP mouse model of Parkinson's disease: critical role for the astrocyte. Proc. Natl. Acad. Sci. U. S. A. 106, 2933-2938.

Cho, Y., Son, H.J., Kim, E.M., Choi, J.H., Kim, S.T., Ji, I.J., Choi, D.H., Joh, T.H., Kim, Y.S., Hwang, O., 2009. Doxycycline is neuroprotective against nigral dopaminergic degeneration by a dual mechanism involving MMP-3. Neurotox Res. 16, 361-371.

Cook, A.L., Vitale, A.M., Ravishankar, S., Matigian, N., Sutherland, G.T., Shan, J., Sutharsan, R., Perry, C., Silburn, P.A., Mellick, G.D., Whitelaw, M.L., Wells, C.A., Mackay-Sim, A., Wood, S.A., 2011. Nrf2 activation restores disease related metabolic deficiencies in olfactory neurosphere-derived cells from patients with sporadic Parkinson's disease. PLoS One. 6, e21907.

Cuadrado, A., Moreno-Murciano, P., Pedraza-Chaverri, J., 2009. The transcription factor Nrf2 as a new therapeutic target in Parkinson's disease. Expert Opin. Ther. Targets. 13, 319-329.

Dauer, W., Przedborski, S., 2003. Parkinson's disease: mechanisms and models. Neuron. 39, 889-909.

de Zeeuw, D., Akizawa, T., Audhya, P., Bakris, G.L., Chin, M., Christ-Schmidt, H., Goldsberry, A., Houser, M., Krauth, M., Lambers Heerspink, H.J., McMurray, J.J., Meyer, C.J., Parving, H.H., Remuzzi, G., Toto, R.D., Vaziri, N.D., Wanner, C., Wittes, J., Wrolstad, D., Chertow, G.M.; BEACON Trial Investigators., 2013. Bardoxolone methyl in type 2 diabetes and stage 4 chronic kidney disease. N. Engl. J. Med. 369, 2492-2503.

Deshmukh, P., Unni, S., Krishnappa, G., Padmanabhan, B., 2017. The Keap1-Nrf2 pathway: promising therapeutic target to counteract ROS-mediated damage in cancers and neurodegenerative diseases. Biophys. Rev. 9, 41-56.

Dong, C., Davis, R.J., Flavell, R.A., 2002. MAP kinases in the immune response. Annu. Rev. Immunol. 20, 55-72.

Drechsel, D.A., Patel, M., 2008. Role of reactive oxygen species in the neurotoxicity of environmental agents implicated in Parkinson's disease. Free Radic. Biol. Med. 44, 1873-1886.

Dumotier, B.M., Deurinck, M., Yang, Y., Traebert, M., Suter, W., 2008. Relevance of in vitro SCREENIT results for drug-induced QT interval prolongation in vivo: a database review and analysis. Pharmacol. Ther. 119, 152-159.

Franklin, K.B.J., Paxinos, G., 1997. *The Mouse Brain in Stereotaxic Coordinates*. Academic Press, San Diego.

Gazaryan, I.G., Thomas, B., 2016. The status of Nrf2-based therapeutics: current perspectives and future prospects. Neural. Regen. Res. 11, 1708-1711.

Guo, X., Han, C., Ma, K., Xia, Y., Wan, F., Yin, S., Kou, L., Sun, Y., Wu, J., Hu, J., Huang, J., Xiong, N., Wang, T., 2019. Hydralazine protects nigrostriatal dopaminergic neurons From MPP+ and MPTP induced neurotoxicity: roles of Nrf2-ARE signaling pathway. Front. Neurol. 10, 271.

Imaizumi, Y., Okada, Y., Akamatsu, W., Koike, M., Kuzumaki, N., Hayakawa, H., Nihira, T., Kobayashi, T., Ohyama, M., Sato, S., Takanashi, M., Funayama, M., Hirayama, A., Soga, T., Hishiki, T., Suematsu, M., Yagi, T., Ito, D., Kosakai, A., Hayashi, K., Shouji, M., Nakanishi, A., Suzuki, N., Mizuno, Y., Mizushima, N., Amagai, M., Uchiyama, Y., Mochizuki, H., Hattori, N., Okano, H., 2012. Mitochondrial dysfunction associated with increased oxidative stress and α-synuclein accumulation in PARK2 iPSC-derived neurons and postmortem brain tissue. Mol. Brain. 5, 35.

Innamorato, N.G., Jazwa, A., Rojo, A.I., García, C., Fernández-Ruiz, J., Grochot-Przeczek, A., Stachurska, A., Jozkowicz, A., Dulak, J., Cuadrado, A., 2010. Different susceptibility to the Parkinson's toxin MPTP in mice lacking the redox master regulator Nrf2 or its target gene heme oxygenase-1. PLoS One. 5, e11838.

Innamorato, N.G., Rojo, A.I., García-Yagüe, A.J., Yamamoto, M., de Ceballos, M.L., Cuadrado, A., 2008. The transcription factor Nrf2 is a therapeutic target against brain inflammation. J. Immunol. 181, 680-689.

Jakel, R.J., Townsend, J.A., Kraft, A.D., Johnson, J.A., 2007. Nrf2-mediated protection against 6-hydroxydopamine. Brain Res. 1144, 192-201.

Kim, S.T., Son, H.J., Choi, J.H., Ji, I.J., Hwang, O., 2010. Vertical grid test and modified horizontal grid test are sensitive methods for evaluating motor dysfunctions in the MPTP mouse model of Parkinson's disease. Brain Res. 1306, 176-183.

Kurkowska-Jastrzebska, I., Wrońska, A., Kohutnicka, M., Członkowski, A., Członkowska, A., 1999. The inflammatory reaction following 1-methyl-4-phenyl-1,2,3,6-tetrahydropyridine intoxication in mouse. Exp. Neurol. 156, 50-61.

Lastres-Becker, I., Ulusoy, A., Innamorato, N.G., Sahin, G., Rábano, A., Kirik, D., Cuadrado, A., 2012. α-Synuclein expression aand Nrf2 deficiency cooperate to aggravate protein aggregation, neuronal death and inflammation in early-stage Parkinson's disease. Hum. Mol. Genet. 21, 3173-3192.

Lee, J.A., Kim, H.R., Kim, J., Park, K.D., Kim, D.J., Hwang, O., 2018a. The novel neuroprotective compound KMS99220 has an early anti-neuroinflammatory effect via AMPK and HO-1, independent of Nrf2. Exp. Neurobiol. 27, 408-418.

Lee, J.A., Kim, J.H., Woo, S.Y., Son, H.J., Han, S.H., Jang, B.K., Choi, J.W., Kim, D.J., Park, K.D., Hwang, O., 2015a. A novel compound VSC2 has anti-inflammatory and antioxidant properties in microglia and in Parkinson's disease animal model. Br. J. Pharmacol. 172, 1087-1100.

Lee, J.A., Son, H.J., Choi, J.W., Kim, J., Han, S.H., Shin, N., Kim, J.H., Kim, S.J., Heo, J.Y., Kim, D.J., Park, K.D., Hwang, O., 2018b. Activation of the Nrf2 signaling pathway and neuroprotection of nigral dopaminergic neurons by a novel synthetic compound KMS99220. Neurochem. Int. 112, 96-107.

Lee, J.A., Son, H.J., Kim, J.H., Park, K.D., Shin, N., Kim, H.R., Kim, E.M., Kim, D.J., Hwang, O., 2016. A novel synthetic isothiocyanate ITC-57 displays antioxidant, anti-inflammatory, and neuroprotective properties in a mouse Parkinson's disease model. Free Radic. Res. 50, 1188-1199.

Lee, J.A., Son, H.J., Park, K.D., Han, S.H., Shin, N., Kim, J.H., Kim, H.R., Kim, D.J.,

Hwang, O., 2015b. A novel compound ITC-3 activates the Nrf2 signaling and provides neuroprotection in Parkinson's disease models. Neurotox. Res. 28, 332-345.

Li, W., Khor, T.O., Xu, C., Shen, G., Jeong, W.S., Yu, S., Kong, A.N., 2008. Activation of Nrf2-antioxidant signaling attenuates NFkappaB-inflammatory response and elicits apoptosis. Biochem. Pharmacol. 76, 1485-1489.

Lu, M.C., Ji, J.A., Jiang, Z.Y., You, Q.D., 2016. The Keap1-Nrf2-ARE pathway as a potential preventive and therapeutic target: an update. Med. Res. Rev. 36, 924-963.

Morse, D., Pischke, S.E., Zhou, Z., Davis, R.J., Flavell, R.A., Loop, T., Otterbein, S.L., Otterbein, L.E., Choi, A.M., 2003. Suppression of inflammatory cytokine production by carbon monoxide involves the JNK pathway and AP-1. J. Biol. Chem. 278, 36993-36998.

Nguyen, L.A., He, H., Pham-Huy, C., 2006. Chiral drugs: an overview. Int. J. Biomed. Sci. 2, 85-100.

Recanatini, M., Poluzzi, E., Masetti, M., Cavalli, A., De Ponti, F., 2005. QT prolongation through hERG K(+) channel blockade: current knowledge and strategies for the early prediction during drug development. Med. Res. Rev. 25, 133-166.

Rojo, A.I., Innamorato, N.G., Martín-Moreno, A.M., De Ceballos, M.L., Yamamoto, M., Cuadrado, A., 2010. Nrf2 regulates microglial dynamics and neuroinflammation in experimental Parkinson's disease. Glia. 58, 588-598.

Rojo, A.I., McBean, G., Cindric, M., Egea, J., López, M.G., Rada, P., Zarkovic, N., Cuadrado, A., 2014. Redox control of microglial function: molecular mechanisms and functional significance. Antioxid. Redox Signal. 21, 1766-1801.

Saito, R., Suzuki, T., Hiramoto, K., Asami, S., Naganuma, E., Suda, H., Iso, T., Yamamoto, H., Morita, M., Baird, L., Furusawa, Y., Negishi, T., Ichinose, M., Yamamoto, M., 2015. Characterizations of three major cysteine sensors of Keap1 in stress response. Mol. Cell Biol. 36, 271-284.

Satoh, T., Lipton, S., 2017. Recent advances in understanding NRF2 as a druggable target: development of pro-electrophilic and non-covalent NRF2 activators to overcome systemic side effects of electrophilic drugs like dimethyl fumarate. F1000Res. 6, 2138.

Scheidereit, C., 2006. IkappaB kinase complexes: gateways to NF-kappaB activation and transcription. Oncogene. 25, 6685-6705.

Schenone, S., Radi, M., Musumeci, F., Brullo, C., Botta, M., 2014. Biologically driven synthesis of pyrazolo[3,4-d]pyrimidines as protein kinase inhibitors: an old scaffold as a new tool for medicinal chemistry and chemical biology studies. Chem. Rev. 114, 7189-7238.

Schindelin, J., Arganda-Carreras, I., Frise, E., Kaynig, V., Longair, M., Pietzsch, T., Preibisch, S., Rueden, C., Saalfeld, S., Schmid, B., Tinevez, J.Y., White, D.J., Hartenstein, V., Eliceiri, K., Tomancak, P., Cardona, A., 2012. Fiji: an open-source platform for biological-image analysis. Nat. Methods. 9, 676-682.

Schmoll, D., Engel, C.K., Glombik, H., 2017. The Keap1-Nrf2 protein-protein interaction: a suitable target for small molecules. Drug Discov. Today Technol. 24, 11-17.

Sierra, A., Gottfried-Blackmore, A.C., McEwen, B.S., Bulloch, K., 2007. Microglia derived from aging mice exhibit an altered inflammatory profile. Glia. 55, 412-424.

Silva, G., Cunha, A., Grégoire, I.P., Seldon, M.P., Soares, M.P., 2006. The antiapoptotic effect of heme oxygenase-1 in endothelial cells involves the degradation of p38 alpha MAPK isoform. J. Immunol. 177, 1894-1903.

Son, H.J., Han, S.H., Lee, J.A., Lee, C.S., Seo, J.W., Chi, D.Y., Hwang, O., 2016. 2-Acetyl-7-hydroxy-6-methoxy-1-methyl-1,2,3,4,-tetrahydroisoquinoline exhibits anti-inflammatory properties and protects the nigral dopaminergic neurons. Eur. J. Pharmacol. 771, 152-161.

Son, H.J., Han, S.H., Lee, J.A., Shin, E.J., Hwang, O., 2017. Potential repositioning of exemestane as a neuroprotective agent for Parkinson's disease. Free Radic. Res. 51, 633-645.

Son, H.J., Lee, J.A., Shin, N., Choi, J.H., Seo, J.W., Chi, D.Y., Lee, C.S., Kim, E.M., Choe, H., Hwang, O., 2012. A novel compound PTIQ protects the nigral dopaminergic neurones in an animal model of Parkinson's disease induced by MPTP. Br. J. Pharmacol. 165, 2213-2227.

Son, H.J., Shin, N., Shin, E.J., Chi, D.Y., Seo, J.W., Lee, C.S., Hwang, O., 2014. AETIQ: a novel synthetic compound with anti-inflammatory properties in activated microglia. Inflammation. 37, 766-774.

Steel, R.J., O'Connell, M.A., Searcey, M., 2018. Perfluoroarene-based peptide macrocycles that inhibit the Nrf2/Keap1 interaction. Bioorg. Med. Chem. Lett. 28, 2728-2731.

Suri, C., Fung, B.P., Tischler, A.S., Chikaraishi, D.M., 1993. Catecholaminergic cell lines from the brain and adrenal glands of tyrosine hydroxylase-SV40 T antigen transgenic mice. J. Neurosci. 13, 1280-1291.

Tu, J., Zhang, X., Zhu, Y., Dai, Y., Li, N., Yang, F., Zhang, Q., Brann, D.W., Wang, R., 2015. Cell-permeable peptide targeting the Nrf2-Keap1 interaction: a potential novel therapy for global cerebral ischemia. J. Neurosci. 35, 14727-14739.

von Otter, M., Bergström, P., Quattrone, A., De Marco, E.V., Annesi, G., Söderkvist, P., Wettinger, S.B., Drozdzik, M., Bialecka, M., Nissbrandt, H., Klein, C., Nilsson, M., Hammarsten, O., Nilsson, S., Zetterberg, H., 2014. Genetic associations of Nrf2-encoding NFE2L2 variants with Parkinson's disease - a multicenter study. BMC Med. Genet. 15, 131.

von Otter, M., Landgren, S., Nilsson, S., Celojevic, D., Bergström, P., Håkansson, A., Nissbrandt, H., Drozdzik, M., Bialecka, M., Kurzawski, M., Blennow, K., Nilsson, M., Hammarsten, O., Zetterberg, H., 2010. Association of Nrf2-encoding NFE2L2 haplotypes with Parkinson's disease. BMC Med. Genet. 11, 36.

Wang, Y.Y., Yang, Y.X., Zhe, H., He, Z.X., Zhou, S.F., 2014. Bardoxolone methyl (CDDO-Me) as a therapeutic agent: an update on its pharmacokinetic and pharmacodynamic properties. Drug Des. Devel. Ther. 8, 2075-2088.

Williamson, T.P., Johnson, D.A., Johnson, J.A., 2012. Activation of the Nrf2-ARE pathway by siRNA knockdown of Keap1 reduces oxidative stress and provides partial protection from MPTP-mediated neurotoxicity. Neurotoxicology. 33, 272-279.

Woo, S.Y., Kim, J.H., Moon, M.K., Han, S.H., Yeon, S.K., Choi, J.W., Jang, B.K., Song, H.J., Kang, Y.G., Kim, J.W., Lee, J., Kim, D.J., Hwang, O., Park, K.D., 2014. Discovery of vinyl sulfones as a novel class of neuroprotective agents toward Parkinson's disease therapy. J. Med. Chem. 57, 1473-1487.

Zhao, Y., Li, J., Gu, H., Wei, D., Xu, Y.C., Fu, W., Y[illegible]., 2015. Conformational preferences of π-π stacking between ligand and protein, analysis derived from crystal structure data geometric preference of π-π interaction. Interdiscip. Sci. 7, 211-220.

Figure captions

Fig. 1: Construction and screening of the pyrazolo [3,4-*d*] pyrimidine library.
(A) Library built with 241 different pyrazolo [3,4-*d*] pyrimidines. (B) Degree of NO downregulation plotted against the degree of HO-1 induction for each compound. (C) Viability (assessed by ATP level) of cells exposed to different concentrations of KKC080106, CDDO-Me, or sulforaphane (SFN). Data are expressed as the percentage relative to the untreated control ± SEM; $^{**}p<0.01$. (D) Cell damage after being exposed to KKC080106 for 24 h; LDH assay (left panel), trypan blue exclusion assay (mid panel), and differential interference contrast microscopy (right panel). Scale bar=100 μm. (E) Synthesis scheme and chemical structure of KKC080106.

Fig. 2: KKC080106 activates Nrf2 and induces the expression of Nrf2 target genes in dopaminergic neurons.
(A) Western blot analysis of Nrf2 in the lysate of CATH.a cells treated with different concentrations of KKC080106 for 24 h. (B) Trypsin-, caspase- and chymotrypsin-like activities of the proteasome exposed to KKC080106 and MG-132 (positive control). Data are expressed as the percentage relative to the untreated control ± SEM; $^{**}p<0.01$, $^{***}p<0.001$. (C) Surface plasmon resonance of Keap1 recorded in the presence of different concentrations of KKC080106; data are expressed as resonance units (RU). (D) Western blot analysis of Nrf2, lamin B (a nuclear marker used as an internal control), and HSP90 (a cytosolic marker used as a negative control) in the nuclear fraction of CATH.a cells treated with KKC080106. (E) RT-PCR analysis of NQO1, HO-1, GCLM, and GCLC using GAPDH as an internal control in CATH.a cells treated with KKC080106. (F) Western blot analysis of NQO1, HO-1, GCLM, and GCLC using β-actin as an internal control in cells treated with KKC080106 for 24 h.

Fig. 3: KKC080106 suppresses the production of proinflammatory molecules and the activation of proinflammatory kinases.
(A) NO levels, (B) IL-1β levels, and (C) TNF-α levels of BV-2 cells exposed to different concentrations of KKC080106 and 0.2 μg/ml LPS. Data are expressed as the percentage relative to the LPS-induced control ± SEM; $^{*}p<0.05$, $^{**}p<0.01$. (D) RT-PCR analysis of iNOS, IL-1β, COX-2, and TNF-α in cells exposed to KKC080106 and 0.2 μg/ml LPS for 6 h. GAPDH was used as an internal control. (E) Western blot analysis of total and phosphorylated IKK and (F) total and phosphorylated MAPKs: JNK, p38 MAPK, and ERK of BV-2 cells treated with KKC080106 and 0.2 μg/ml LPS.

Fig. 4: KKC080106 prevents the nigrostriatal neurodegeneration and suppresses microglial activation in MPTP-treated mice.

(A) Photomicrographs of the nigral (left) and striatal (right) sections immunostained against TH (Scale bar=200 μm). (B) Number of TH-immunopositive neurons in the SN. (C) Immunodensity of TH-stained terminals in the striatum. (D) Photomicrographs of the nigral sections against Iba-1 (Scale bar=150 μm). (E) Immunodensity of Iba-1-stained microglia in the SN. Data are expressed as percentage relative the control group ± SEM; $^{**}p<0.01$.

Fig. 5: KKC080106 alleviates motor deficits of MPTP-treated mice.

(A) Hindlimb test score. (B) Latent time on rotarod. (C) Sum of step distances on the horizontal grid. (D) Total number of successful steps made on the horizontal grid. (E) Time taken to climb down the vertical grid. (F) Time taken to make a turn on the vertical grid. (G) Total time taken on the vertical grid. (H) Percentage of successful steps made on the vertical grid. Data are expressed as mean ± SEM; $^{*}p<0.05$, $^{**}p<0.01$.

Table 1: Evaluation of KKC080106 toxicity after a single administration. Acute toxicity was evaluated in Sprague-Dawley rats (n=3) following a single oral administration of different doses of KKC080106. Animals were observed daily for 14 days, after which they were euthanized with CO_2.

Administered	**Injection volume (ml/kg)**	**Dose (mg/kg)**	**Mortality**	**General signs of toxicity**
vehicle	20	0	0	None
KKC080106	20	500	0	None
	20	1,000	0	None
	20	2,000	0	None

Table 2: Stability of KKC080106 against plasma enzymes. KKC080106 was incubated with plasma enzyme preparations from human, dog, rat, and mouse for different time periods. The remaining KKC080106 at each time point was measured by LC-MS/MS analysis. Data are expressed as mean±SEM of two independent experiments.

Time (h)	Human (%)	Dog (%)	Rat (%)	Mouse (%)
0.0	100.0 ± 15.1	100.0 ± 17.0	100.0 ± 28.8	100.0 ± 29.7
0.5	104.0 ± 24.6	89.7 ± 21.5	58.4 ± [illegible]4.9	109.2 ± 22.0
1.0	93.5 ± 19.2	95.6 ± 30.8	46.[illegible] ± [illegible]3.7	99.0 ± 2.3
2.0	86.8 ± 5.1	84.2 ± 24.1	[illegible] ± 13.6	96.9 ± 11.1
6.0	85.5 ± 4.3	78.8 ± 24.2	[illegible] ± 14.9	74.9 ± 6.2

Table 3: Pharmacokinetic parameters of KKC080106 in mouse plasma and brain. Mice (n=3) were administered 5 mg/kg via intravenous (iv) injection and 10 mg/kg via oral (po) gavage.

Parameters	**iv**		**po**	
	Plasma	**Brain**	**Plasma**	**Brain**
AUC_{0-24} (ng·h/ml)	2,089.4	551.9	2,387.9	363.0
C_{max} (ng/ml)			1,061.0	111
T_{max} (h)			0.5	1.0
BA (%)	57			
Brain Distribution (%)	26		15	

AUC = area under the plasma concentration-time curve, C_{max} = maximum concentration of the drug; T_{max} = time taken to reach C_{max}; Bioavailability (BA) = (AUC_{po}/AUC_{iv}) x 100; Brain distribution (%) = (AUC_{brain}/AUC_{plasma}) x 100.

Table 4: Pharmacokinetic parameters of KKC080106 in rat plasma and brain. Rats (n=3) were administered 1.25 mg/kg via intravenous (iv) injection and 10 mg/kg via oral (po) gavage.

Parameters	**iv**		**po**	
	Plasma	**Brain**	**Plasma**	**Brain**
AUC_{0-24} (ng·h/ml)	572.3	246.2	1,576.5	589.7
C_{max} (ng/ml)			373.1	114.5
T_{max} (h)			1.0	1.0
BA (%)	34			
Brain Distribution (%)	43		37	

AUC = area under the plasma concentration-time curve, C_{max} = maximum concentration of the drug; T_{max} = time taken to reach C_{max}; Bioavailability (BA) = (AUC_{po}/AUC_{iv}) x 100; Brain distribution (%) = (AUC_{brain}/AUC_{plasma}) x 100.

Highlights

• KKC080106 was selected from a pyrazolo[3,4-*d*]pyrimidine library we constructed.

• It binds to Keap1, activates Nrf2 and elevates Nrf2 target gene expression.

• It suppresses the inflammatory signaling and production of the inflammatory markers.

• It prevents MPTP-induced neurodegeneration, microglial activation and motor deficits.

• It exhibits good safety and pharmacokinetic profiles as a CNS drug.

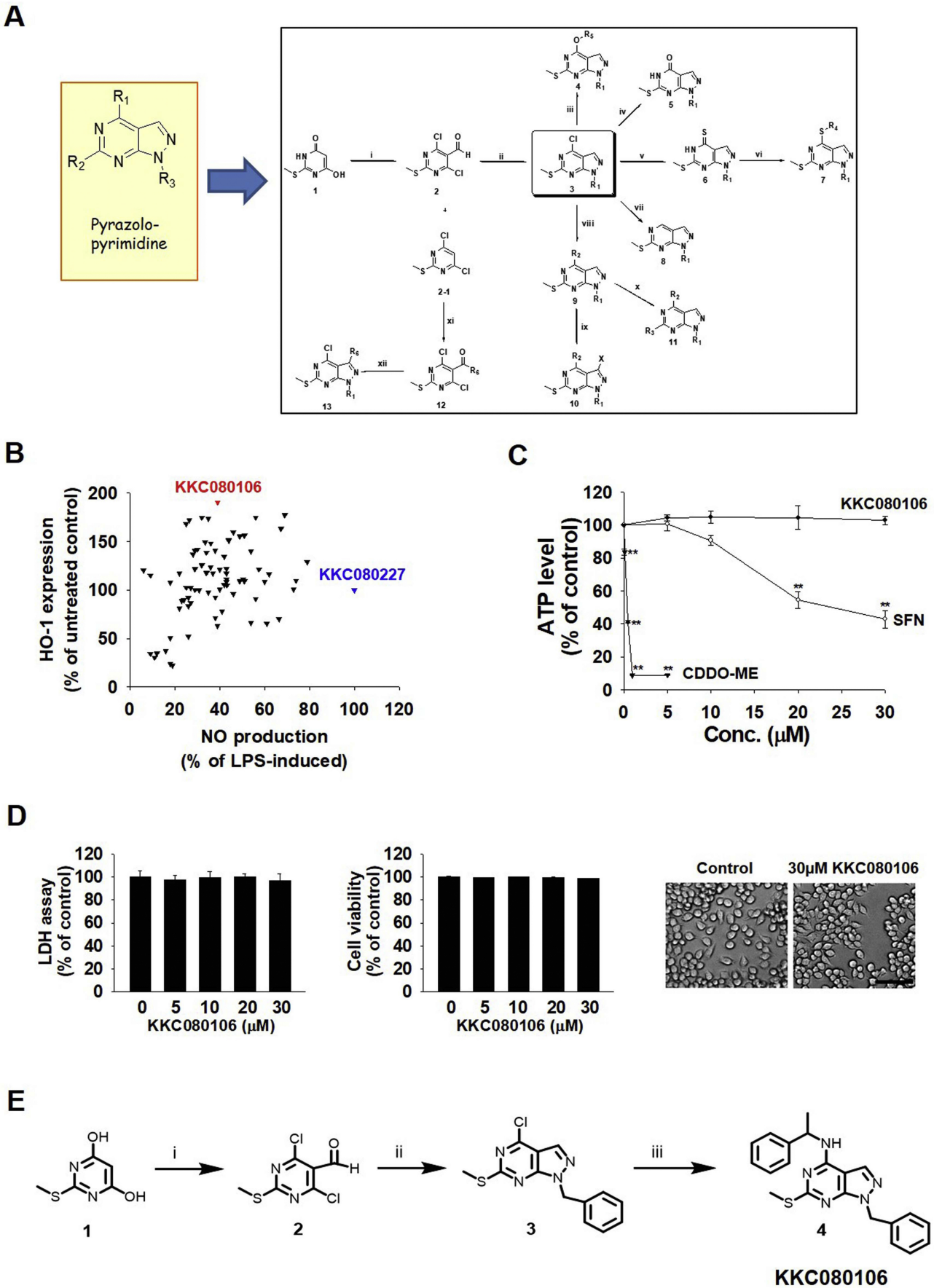
A
Pyrazolo-
pyrimidine
B
KKC080106
KKC080227
HO-1 expression
(% of untreated control)
NO production
(% of LPS-induced)
C
KKC080106
SFN
CDDO-ME
ATP level
(% of control)
Conc. (μM)
D
LDH assay
(% of control)
KKC080106 (μM)
Cell viability
(% of control)
KKC080106 (μM)
Control
30μM KKC080106
E
1
2
3
4
KKC080106

Figure 1

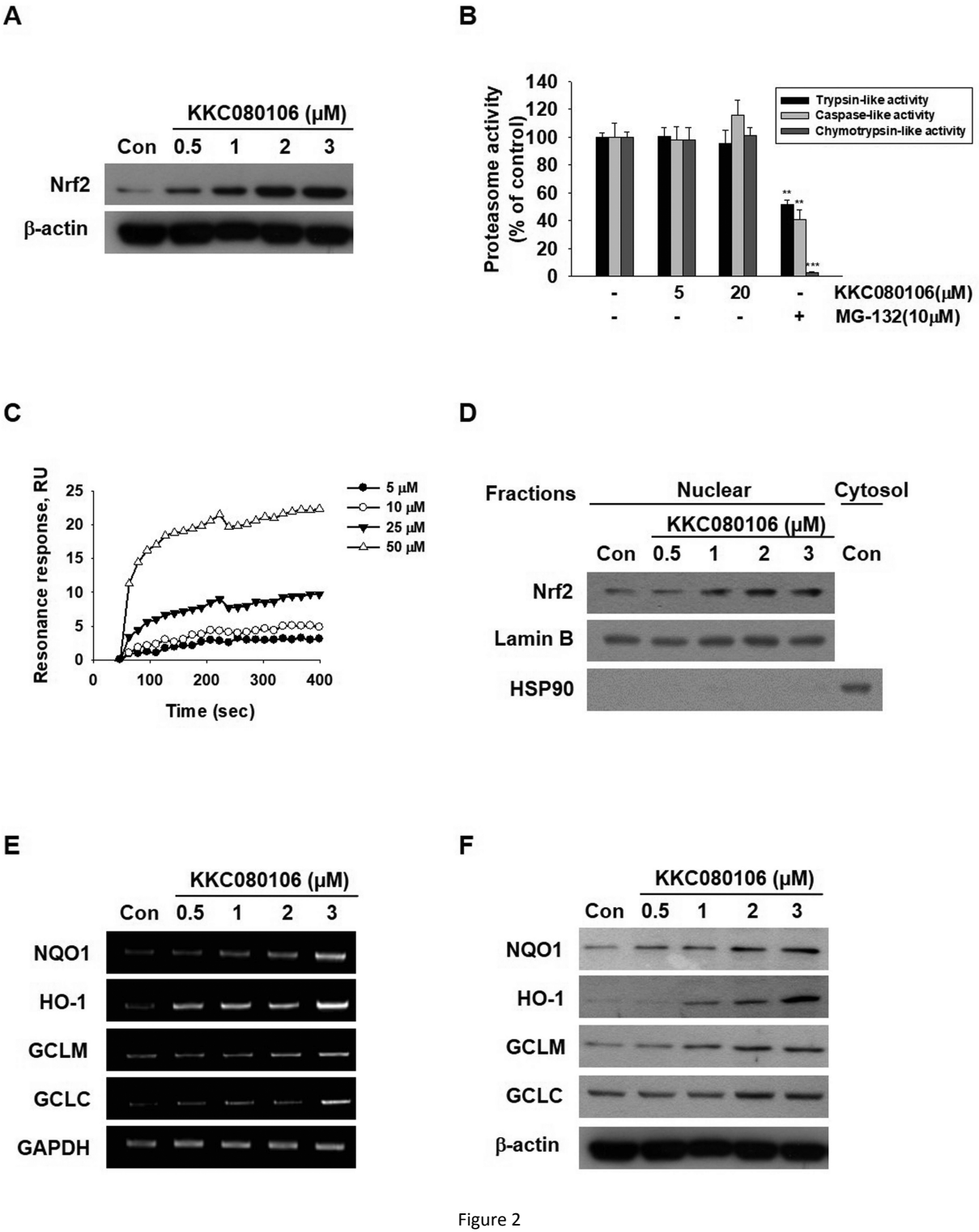
A
KKC080106 (μM)
Con 0.5 1 2 3
Nrf2
β-actin
B
Proteasome activity (% of control)
140
120
100
80
60
40
20
0
Trypsin-like activity
Caspase-like activity
Chymotrypsin-like activity
**
**
**
- 5 20 - KKC080106(μM)
- - - + MG-132(10μM)
C
Resonance response, RU
25
20
15
10
5
0
0 100 200 300 400
Time (sec)
5 μM
10 μM
25 μM
50 μM
D
Fractions
Nuclear
Cytosol
KKC080106 (μM)
Con 0.5 1 2 3 Con
Nrf2
Lamin B
HSP90
E
KKC080106 (μM)
Con 0.5 1 2 3
NQO1
HO-1
GCLM
GCLC
GAPDH
F
KKC080106 (μM)
Con 0.5 1 2 3
NQO1
HO-1
GCLM
GCLC
β-actin

Figure 2

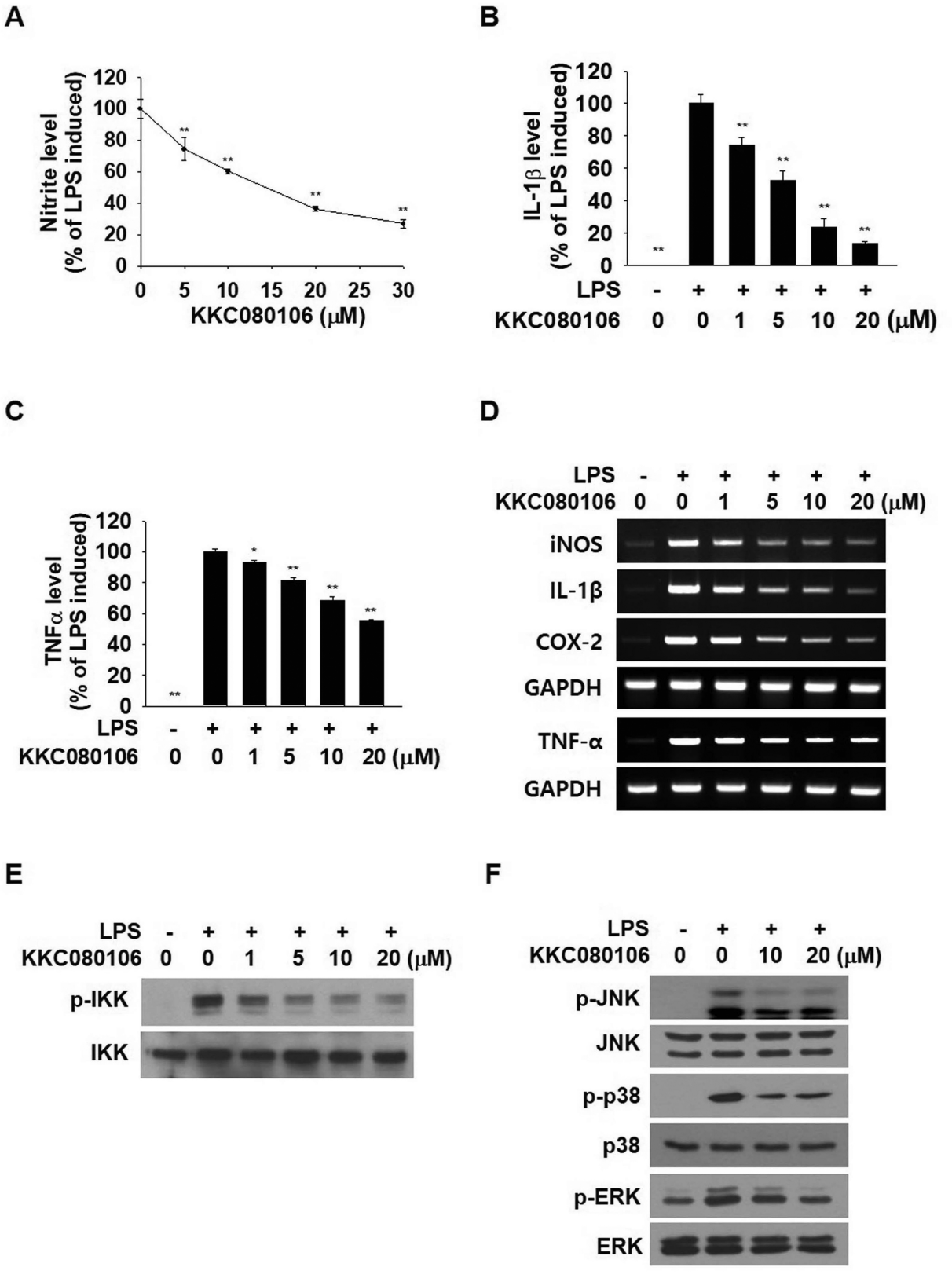
A
Nitrite level (% of LPS induced)
120
100
80
60
40
20
0
0 5 10 15 20 25 30
KKC080106 (μM)
B
IL-1β level (% of LPS induced)
LPS - + + + + +
KKC080106 0 0 1 5 10 20 (μM)
C
TNFα level (% of LPS induced)
LPS - + + + + +
KKC080106 0 0 1 5 10 20 (μM)
D
LPS - + + + + +
KKC080106 0 0 1 5 10 20 (μM)
iNOS
IL-1β
COX-2
GAPDH
TNF-α
GAPDH
E
LPS - + + + + +
KKC080106 0 0 1 5 10 20 (μM)
p-IKK
IKK
F
LPS - + + +
KKC080106 0 0 10 20 (μM)
p-JNK
JNK
p-p38
p38
p-ERK
ERK

Figure 3

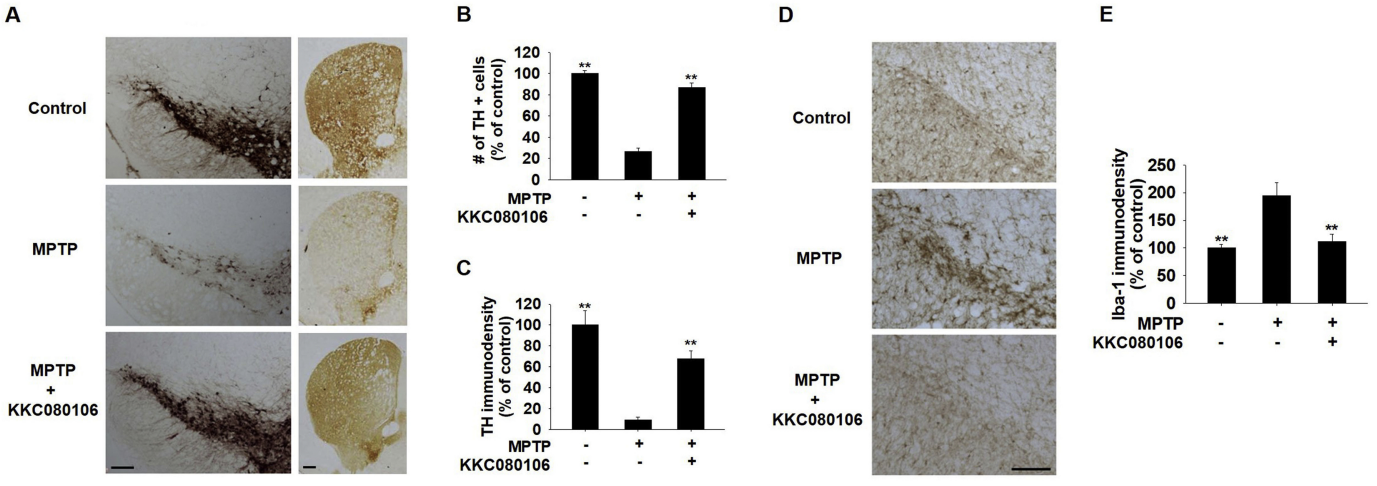
A
Control
MPTP
MPTP
+
KKC080106
B
# of TH + cells
(% of control)
120
100
80
60
40
20
0
**
**
MPTP - + +
KKC080106 - - +
C
TH immunodensity
(% of control)
120
100
80
60
40
20
0
**
**
MPTP - + +
KKC080106 - - +
D
Control
MPTP
MPTP
+
KKC080106
E
Iba-1 immunodensity
(% of control)
250
200
150
100
50
0
**
**
MPTP - + +
KKC080106 - - +

Figure 4

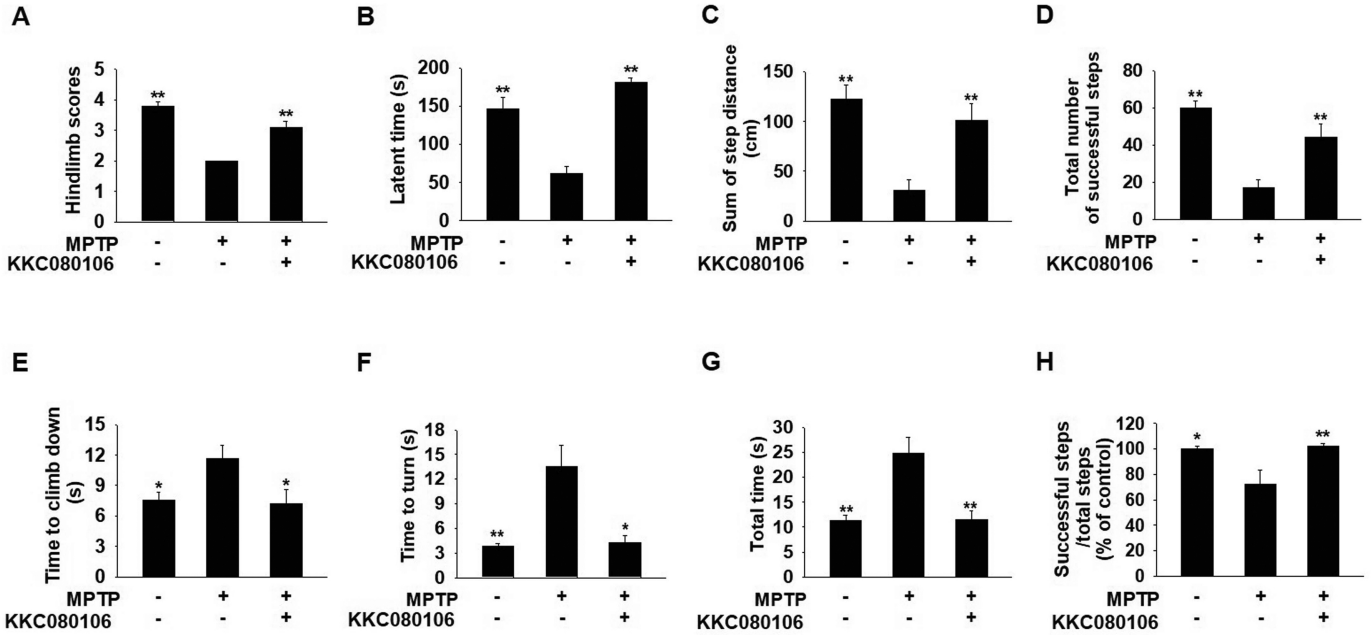
A
Hindlimb scores
B
Latent time (s)
C
Sum of step distance (cm)
D
Total number of successful steps
E
Time to climb down (s)
F
Time to turn (s)
G
Total time (s)
H
Successful steps /total steps (% of control)
MPTP
KKC080106

Figure 5